SCIENTIFIC REPORTS

OPEN

SUBJECT AREAS:
CONDENSED-MATTER PHYSICS
MATERIALS SCIENCE
APPLIED PHYSICS
SPINTRONICS

Received
2 May 2012

Accepted
10 October 2012

Published
12 December 2012

Correspondence and requests for materials should be addressed to S.-C.S. (scshin@kaist.ac.kr; scshin@dgist.ac.kr)

Thermal spin injection and accumulation in CoFe/MgO/*n*-type Ge contacts

Kun-Rok Jeon[1], Byoung-Chul Min[2], Seung-Young Park[3], Kyeong-Dong Lee[1], Hyon-Seok Song[1], Youn-Ho Park[2], Young-Hun Jo[3] & Sung-Chul Shin[1,4]

[1]Department of Physics and Center for Nanospinics of Spintronic Materials, Korea Advanced Institute of Science and Technology (KAIST), Daejeon 305-701, Korea, [2]Center for Spintronics Research, Korea Institute of Science and Technology (KIST), Seoul 136-791, Korea, [3]Nano Materials Research Team, Korea Basic Science Institute (KBSI), Daejeon 305-764, Korea, [4]Department of Emerging Materials Science, Daegu Gyeongbuk Institute of Science and Technology (DGIST), Daegu 711-873, Korea.

Understanding the interplay between spin and heat is a fundamental and intriguing subject. Here we report thermal spin injection and accumulation in CoFe/MgO/*n*-type Ge contacts with an asymmetry of tunnel spin polarization. Using local heating of electrodes by laser beam or electrical current, the thermally-induced spin accumulation is observed for both polarities of the temperature gradient across the tunnel contact. We observe that the magnitude of thermally injected spin signal scales linearly with the power of local heating of electrodes, and its sign is reversed as we invert the temperature gradient. A large Hanle magnetothermopower (HMTP) of about 7.0% and the Seebeck spin tunneling coefficient of larger than 0.74 meV K^{-1} are obtained at room temperature.

The tremendous power consumption and accompanying heat generation in current electronic devices requires alternative technologies to provide a solution for the energy issues and to realize the energy efficient electronics. Spintronics is a viable route for it, using the spin degree of freedom in addition to the conventional charge transport[1]. Recently another important ingredient, namely heat, appears on the stage. It has been reported that the temperature gradient and heat flow in ferromagnetic structures gives rise to a variety of spin related phenomena[2]. Understanding the interplay between heat and spin transport is a fundamental and intriguing subject but also offers unique possibilities for emerging electronics based on the combination of thermoelectrics and spintronics.

Especially in SC-based spintronics, the functional use of heat provides a new route to inject and control of spin in semiconductors (SCs)[3]. The generation of non-equilibrium spin populations (*i.e.* spin accumulation) in nonmagnetic SC is a central issue of SC-based spintronics[1,3–5]. Significant progress has been made on the spin accumulation in various SC systems by means of circularly polarized light[4,6], spin-polarized tunneling[7–13], hot-electron spin filtering[14,15], spin-orbit interaction[16,17], or magnetization dynamics[18,19].

Intriguingly, Le Breton *et al.*[20] have reported a rather different mechanism for the spin accumulation, in which temperature difference across a ferromagnet (FM)/oxide/SC tunnel contact can induce the spin accumulation ($\Delta\mu$) in SC via Seebeck spin tunneling (SST). It was found that the SST effect, involving thermal transfer of spin angular momentum from FM to SC without a tunneling charge current, is a purely interface-related phenomenon of the tunnel contact and governed by the energy dependence of its tunnel spin polarization (TSP)[20]. This provides a conceptually new mechanism for the generation of $\Delta\mu$ in SC as well as for the functional use of heat in spintronic devices[20]. The SST and thermal spin accumulation ($\Delta\mu_{th}$) in *p*-type SC (e.g., *p*-type Si) have been intensely studied, using a $Ni_{80}Fe_{20}/Al_2O_3/SiO_2/p$-SC contact with the asymmetry in TSP of tunneling holes[20]. However, the counterpart of *n*-type SC still needs to be explored[21].

Here we report the thermal spin injection and accumulation in *n*-type Ge by employing CoFe/MgO/Ge contacts with the asymmetry in TSP of tunneling electrons. The Joule heating of Ge by electrical current or local heating of CoFe electrode by a laser beam gives rise to a temperature gradient across the tunnel contact and a consequent thermal spin injection into Ge. The thermally-induced spin accumulation was detected by means of the Hanle effect. The sign and magnitude of Hanle signals are analyzed using spin-dependent tunneling theory.

Results

Principle of the approach. Figures 1a and 1b illustrate the thermal spin injection and accumulation process in a FM/oxide/SC tunnel contact for the case that the temperature of SC (T_{SC}) is higher than the temperature of FM

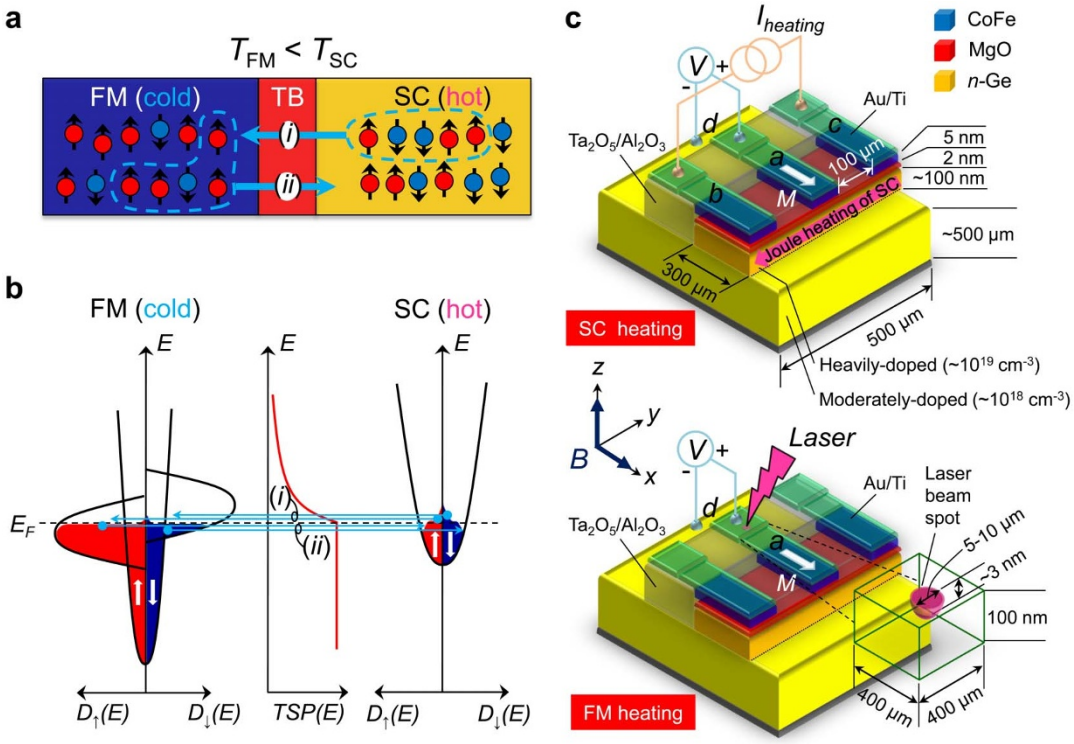

Figure 1 | Principle of the approach. (a) Schematic illustration of SST process in a FM/oxide/SC tunnel contact for the case that temperature of SC is larger than that of FM. (b) Spin-dependent density of states and its occupation for the tunnel contact with a hot SC and a cold FM. The representative profile of TSP vs. E for the CoFe/MgO/n-Ge contact is schematically illustrated on the middle. The (i) and (ii) represent, respectively, the forward and reverse tunneling processes of electrons driven by the temperature difference. (c) Device geometry and measurement scheme.

(T_{FM})[20]. The temperature difference results in the unequal electron distributions in the FM and SC; the hot SC has a relatively larger number of filled (empty) states above (below) the Fermi-level (E_F) than those of the cold FM (see Fig. 1b). Consequently, the electrons above E_F mainly tunnel from the SC into FM (forward tunneling, indicated as (i) in Figs. 1a and 1b), and the electrons below E_F flow in the opposite direction (reverse tunneling, indicated as (ii) in Figs. 1a and 1b). The important feature of the SST process is that the numbers of electrons tunneling in the opposite direction are the same, and there is no net charge current. Nevertheless, if the energy dependence of TSP are different for the forward and reverse tunneling (in other words, the Seebeck tunnel coefficient for majority and minority spin electrons are different), a spin accumulation (or $\Delta\mu_{th}$) can be induced in the SC[20]. Obviously, the sign of $\Delta\mu_{th}$ can be reversed when the temperate gradient is inverted; the cold SC has a relatively smaller number of filled (empty) states above (below) the Fermi-level (E_F) than those of the hot FM.

Figure 1c shows the device geometry and measurement scheme used in the present study. We fabricated a symmetric device consisting of three epitaxial CoFe(5 nm)/MgO(2 nm)/n-Ge tunnel contacts (a–c, 100×300 μm^2) where the n-Ge channel is composed of a heavily P-doped surface layer ($n_d \sim 10^{19}$cm^{-3}at 300 K) and a moderately Sb-doped substrate ($n_d \sim 10^{18}$cm^{-3}at 300 K). These contacts are separated by about 100 μm from each other, which is much longer than the spin diffusion length. The magnetic easy axis of the CoFe contacts are along the [110] direction of Ge in parallel to the long axes of the contacts. Details of the structural and electrical characterizations can be found elsewhere[22,23].

To effectively generate the temperature difference ($\Delta T \equiv T_{Ge} - T_{CoFe}$) in the tunnel contact a, we used two different heating methods. For the SC heating (top panel of Fig. 1c), we applied a heating current ($I_{heating}$) through the SC channel using two contacts b and c, which causes Joule heating and raises T_{Ge} with respect to T_{CoFe} ($\Delta T > 0$). For the FM heating (bottom panel of Fig. 1c), the Au bond pad was heated using a laser beam with a wavelength of 532 nm and a maximum power of 200 mW (note that the results obtained with the Joule heating of FM are shown in the Supplementary Information Note I). The laser beam spot (with a diameter of 5–10 μm and a skin depth of ~3 nm) on the 100 nm-thick Au pad is located at around 300 μm from the one edge of the tunnel contact. The size of the Au pad is large enough to prevent the direct illumination of the Ge layer. A part of heat generated from the laser beam passes through the contact, resulting in $T_{CoFe} > T_{Ge}$ ($\Delta T < 0$).

In an open-circuit geometry, where the tunneling charge current (I_{tunnel}) is zero, the measured voltage between the contact a and d is given by $V = V_{th} + \Delta V_{TH}$[20]. The first term V_{th} is the thermovoltage maintaining zero net charge current (I_{tunnel}=0) and the second term ΔV_{TH} is the SST voltage due to the induced $\Delta\mu_{th}$ in the SC. The ΔV_{TH} can be detected by means of the Hanle effect[24,25]. When we apply magnetic fields (B_z) transverse to the spins in the SC, the $\Delta\mu_{th}$ is suppressed via spin precession. This results in a voltage change (ΔV_{TH}), directly proportional to $\Delta\mu_{th}$, with a Lorentzian line shape as a function of the B_z. These two measurement schemes (Fig. 1c) using the Hanle effect[24,25] provide a concrete means of demonstrating the SST and resultant $\Delta\mu_{th}$ in the SC.

Energy dependence of tunnel spin polarization in the CoFe/MgO/*n*-Ge contact. Before conducting the thermal spin injection experiments, we have estimated the form of TSP as a function of E, which determine the sign and magnitude of induced $\Delta\mu_{th}$, using the conventional three-terminal Hanle (TTH) measurement[7,20,26]. Instead of applying $I_{heating}$, a non-zero I_{tunnel} (or I_{ac}) is applied across the contact a and c of the CoFe/MgO/n-Ge contact while the V is measured using the contact a and d in an applied magnetic field (see Fig. 1c).

Figure 2a shows the results obtained from the TTH measurements (up to 4 kOe) under perpendicular (B_z, closed circles) and in-plane

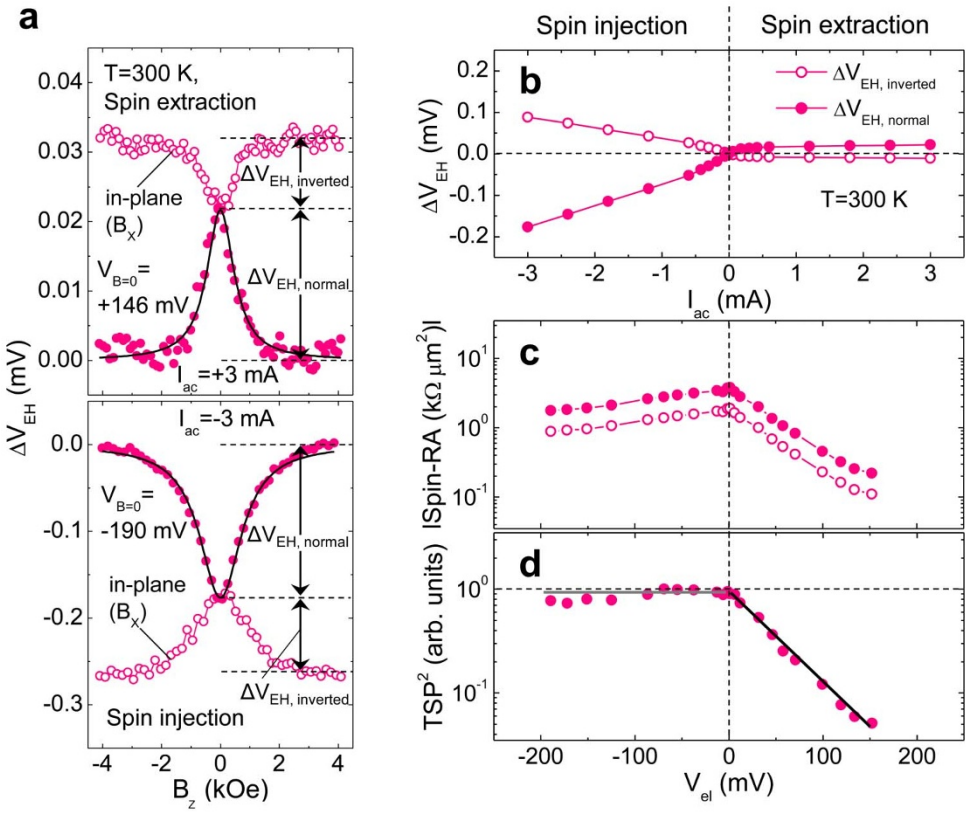

Figure 2 | Energy dependence of tunnel spin polarization for the CoFe/MgO/*n*-Ge contact. (a) TTH measurements (up to 4 kOe) for the CoFe/MgO/*n*-Ge contact under perpendicular (B_z, closed circles) and in-plane (B_x, open circles) magnetic fields at 300 K. (b) Electrical Hanle signals ($\Delta V_{EH,\ normal}$ and $\Delta V_{EH,\ inverted}$) as a function of an applied current (I_{ac}) at 300 K. (c) Corresponding spin RA products ($\Delta V_{EH,\ normal}/J_{ac}$ and $\Delta V_{EH,\ inverted}/J_{ac}$) and (d) estimated TSP^2 for $\Delta V_{EH,\ normal}/J_{ac}$ with a bias voltage ($V_{el} = V_{CoFe} - V_{Ge}$), defined as $V_{B=0} - \Delta V_{EH}$.

(B_x, open circles) magnetic fields at RT. Clear electrical Hanle signals (ΔV_{EH}) with a Lorentzian line shape are detected at RT. It should be noted that the full spin accumulation ($\Delta\mu$) consists of the inverted Hanle signal ($\Delta V_{EH,\ inverted}$) in B_x and the normal Hanle signal ($\Delta V_{EH,\ normal}$) in B_z[27,28]. As shown in Figs. 2a and 2b, the electrical Hanle signals (ΔV_{EH}) are significantly asymmetric with respect to the bias polarity, which is consistent with the previous work[23]. Both the $\Delta V_{EH,\ normal}$ and $\Delta V_{EH,\ inverted}$ increase linearly with increasing the reverse bias current ($I_{ac} < 0$, electron spin injection), but change slightly with increasing the forward bias current ($I_{ac} > 0$, electron spin extraction). This asymmetry can also be seen in the middle panel of Fig. 2c, where the spin-RA products ($\Delta V_{EH}/J_{ac}$) is plotted as a function of the electrical voltage ($V_{el} = V_{CoFe} - V_{Ge}$). It should be mentioned here that the obtained spin-RA value (2–3 k$\Omega\,\mu m^2$) is several orders of magnitude larger than the expected value from the existing spin injection and diffusion theory[5]. This discrepancy between experiment and theory in the TTH measurement has been consistently observed with many types of tunnel barrier and SC, as discussed in the Ref. 3. The origins of this discrepancy, other enhancement factors not yet incorporated in the existing theory, are still under investigation[29].

According to the spin injection and diffusion theory[5], the $\Delta V_{EH,\ normal}/J_{ac}$ is proportional to $\gamma_d\gamma_{i/e}\sqrt{\tau_{sf}}$ at a given temperature (T), which depends on V_{el} (note that, although the existing theory does not provide the quantitative agreement with the experiment, it provides the qualitative description of the TSP^2 variation with E). Here, the γ_d is the TSP corresponding to the detection of induced spin accumulation at the Ge interface, the $\gamma_{i/e}$ is the TSP of the injected/extracted electrons, and the τ_{sf} is the spin lifetime. Using the $\Delta V_{EH,\ normal}/J_{ac}$ values (Fig. 2c) and effective (τ_{sf}) values (not shown) extracted from the Lorentzian fit (black line in Fig. 2a), we plotted the TSP^2 ($\gamma_d\gamma_{i/e}$, normalized) vs. V_{el} in Fig. 2d. With the assumption of $\gamma_d = \gamma_{i/e}$, the variation of TSP (γ) with E is then obtained as $\gamma(E) \propto \gamma_o$ for $E < E_F$ (gray line in Fig. 2d) and $\gamma(E) \propto \gamma_o \exp(-(E-E_F)/0.1)$ for $E > E_F$ (black line in Fig. 2d). The estimated profile of TSP vs. E is indeed similar to the schematically illustrated one on the middle panel of Fig. 1b. This asymmetry in the TSP of CoFe/MgO/*n*-Ge contacts is essential to induce the large $\Delta\mu_{th}$ in Ge via the SST[20].

Detection of thermal spin accumulation in Ge. The SST and resultant $\Delta\mu_{th}$ in Ge were detected in the measurement geometry shown in the top panel of Fig. 1c. While heating the Ge side ($\Delta T > 0$) as described above, the voltage change ($\Delta V_{TH} \propto \Delta\mu_{th}$) is measured as a function of the applied magnetic field (B_z, B_x).

As shown the ΔV_{TH}-B_z plots in Figs. 3a and 3b, significant normal Hanle signals ($\Delta V_{TH,\ normal}$) with the Lorentzian line shape similar to that of ΔV_{EH} (see Fig. 2a) were observed at 300 K. The inverted Hanle signals ($\Delta V_{TH,\ inverted}$)[27,28] in B_x (Figs. 3c and 3d), roughly half the magnitude of the $\Delta V_{TH,\ normal}$, were also clearly measured.

The magnitude of thermal Hanle signals (ΔV_{TH}) as a function of the $I_{heating}$ (up to ± 10 mA) is summarized in Figs. 3e–3h. In these figures, we can clearly see that the $\Delta V_{TH,\ normal}$ and also $\Delta V_{TH,\ inverted}$ scale quadratically with the $I_{heating}$, and scale linearly with the heating power density ($P_{heating}$). The $P_{heating}$ is proportional to $R_{Ge}I^2_{heating}/L^{Ge}_x L^{Ge}_y L^{Ge}_z$, where the R_{Ge} is the resistance of the Ge heating layer and the $L^{Ge}_x L^{Ge}_y L^{Ge}_z$ is its volume. These results strongly support that the observed signals mainly come from the thermally driven spin accumulation, which scales linearly with the ΔT[20,30], in Ge.

The sign of $\Delta\mu_{th}$ has been determined by a direct comparison with that of ΔV_{EH} obtained from the TTH measurements for the same tunnel contact a[20]. The sign of $\Delta V_{EH,\ normal}$ is negative for

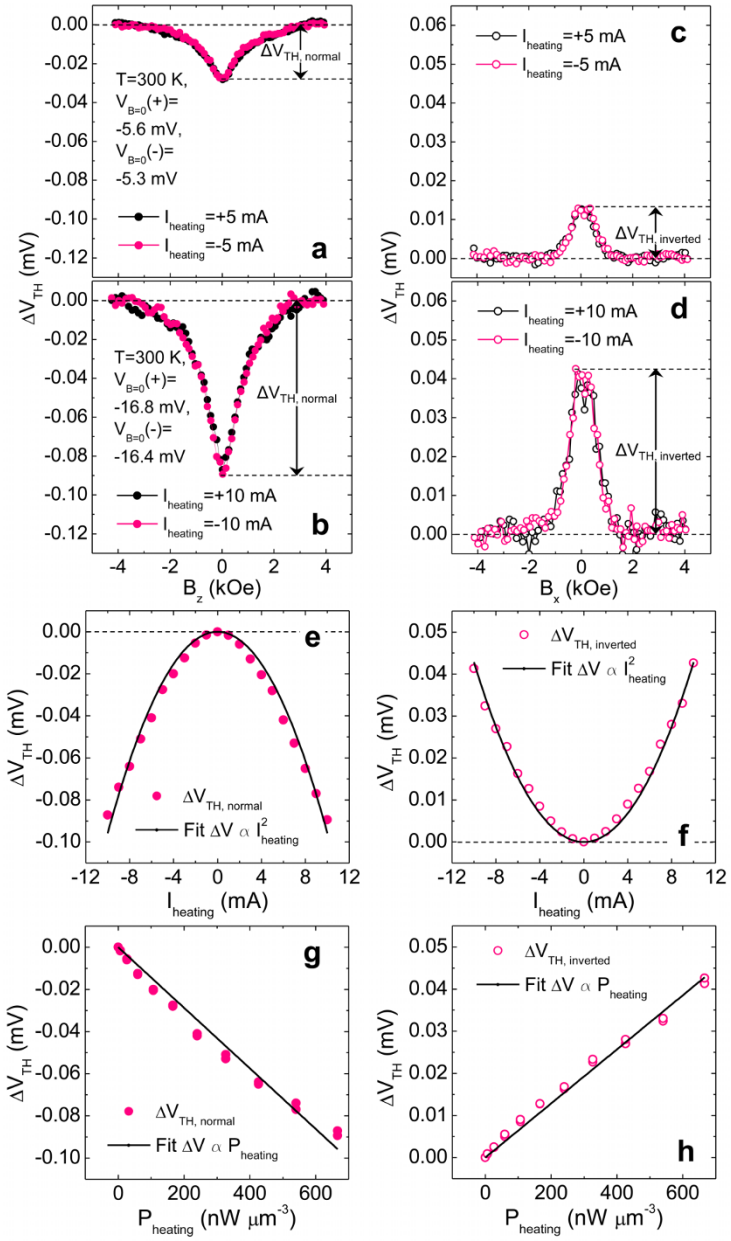

Figure 3 | Detection of thermal spin accumulation in Ge with heating SC. Thermal Hanle signals ($\Delta V_{TH,\ normal}$, $\Delta V_{TH,\ inverted}$) in applied magnetic fields (B_z, closed circles; B_x, open circles) for heating currents ($I_{heating}$) of ± 5 and ± 10 mA at 300 K. (a)/(b) and (c)/(d) represent $\Delta V_{TH,\ normal}$ and $\Delta V_{TH,\ inverted}$ for $I_{heating}$ of $\pm 5/\pm 10$ mA, respectively. (e) $\Delta V_{TH,\ normal}$ and (f) $\Delta V_{TH,\ inverted}$ with the $I_{heating}$ (up to ± 10 mA), together with a quadratic fit. (g) $\Delta V_{TH,\ normal}$ and (h) $\Delta V_{TH,\ inverted}$ with the $P_{heating}$, together with a linear fit.

negative V_{el} ($V_{CoFe} - V_{Ge} < 0$, electron spin injection) and positive for positive V_{el} ($V_{CoFe} - V_{Ge} > 0$, electron spin extraction) in Figs. 2(a) and (b). The $\Delta V_{TH,\ normal}$ in Figs. 3a and 3b has the same sign with the former $\Delta V_{EH,\ normal}$ ($V_{el} < 0$), which means that the $\Delta\mu_{th}$ produced by the thermal spin injection has the same sign as the $\Delta\mu_{el}$ induced by the electrical spin injection. Given the positive TSP of epitaxial bcc FM/MgO(001) tunnel interfaces[31,32], the $\Delta\mu_{th}$ induced by the SST for $T_{Ge} > T_{CoFe}$ corresponds to the majority spin accumulation ($\Delta\mu > 0$) in the Ge. This is in agreement with the expected $\Delta\mu_{th}$ from the SST mechanism[20]: when the TSP of FM/oxide/SC contacts (with positive sign) is constant below E_F but decay above E_F, as shown in Figs. 1b and 2d, majority spins accumulate in the SC ($\Delta\mu > 0$) for $T_{Ge} > T_{CoFe}$ (see Figs. 1a and 1b). We have calculated that the induced $\Delta\mu_{th}$ is (+)0.26 meV with the maximum $P_{heating}$ (667 nW μm^{-3}) from $\Delta\mu_{th} = (-2e)\Delta V_{TH}/\gamma$[3,5,20], using the measured $\Delta V_{TH,\ normal}$ of (–)0.09 mV and the assumed TSP (γ) of (+)0.7 for the epitaxial CoFe/MgO tunnel interface[31,32]. This value should be considered as a lower limit for the $\Delta\mu_{th}$, since we used the highest value of TSP. The SST theory[20] based on the free-electron model predicts the $\Delta\mu_{th}$ value of ~10 μeV for the ΔT of ~1 K. Considering the possible range of ΔT across the tunnel contact is from 0.15 mK to 350 mK (see the Supplementary Information Note II), the obtained signal is at least one order of magnitude larger than the predicted value, which was also observed in the $Ni_{80}Fe_{20}/Al_2O_3/SiO_2/p$-Si contact[20]. It is probably due to the limitation of the free-election model, the lack of detailed information about the energy dependence of TSP near the E_F, and the ignorance of inelastic (magnon-assisted) spin tunneling[20].

It should be mentioned that our system requires about 100 times larger $P_{heating}$ to obtain a similar magnitude of ΔV_{TH} compared to the silicon-on-insulator (SOI) wafer based system[20]. This is mainly attributed to the different device structure. In our device structure,

the ΔT across the tunnel contact is small because a large part of the Joule heat produced in the heavily-doped Ge layer can flow away to the substrate. The calculated heat flow ratio (R_Q^{tunnel}) across the tunnel barrier in our device is more than one order of magnitude smaller than that in the SOI wafer based device[20] (see the Supplementary Information Note II).

Sign reversal of thermal spin signal by reversing the temperature difference. Another important feature of SST and $\Delta\mu_{th}$ is that the sign of the thermal spin signal is reversed when ΔT is reversed. To demonstrate this, we employed a laser beam for heating the FM instead of the Joule heating method. This approach allows us to heat the FM ($\Delta T<0$) effectively and exclude the contribution of spurious effects such as the current-in-plane (CIP) tunneling and anisotropic magnetoresistance (AMR) on the Hanle signal (see the Supplementary Information Note I).

Figures 4a and 4b show the obtained thermal spin signals as a function of perpendicular (B_z, Fig. 4a) and in-plane (B_x, Fig. 4b) magnetic fields with varying the laser power density (P_{laser}) at RT ($\Delta T<0$). It should be noticed that we used the same contact *a* (see Fig. 1c) in both cases of the SC and FM heating. Clear normal and inverted Hanle signals are observed and the amplitudes of both Hanle signals are gradually increased with increasing the P_{laser}. As shown in the ΔV_{TH}-P_{laser} plots (Figs. 4c and 4d), the obtained Hanle signals ($\Delta V_{TH,\,normal}$ and $\Delta V_{TH,\,inverted}$) scale almost linearly with the P_{laser}, indicating that the obtained signal is from the thermal spin injection and accumulation in Ge.

We can see that the sign of ΔV_{TH} is apparently reversed with respect to the SC heating case: the $\Delta V_{TH,\,normal}$ ($\Delta V_{TH,\,inverted}$) is positive (negative) for $T_{CoFe}>T_{Ge}$ (see Figs. 4c and 4d) whereas it is negative (positive) for $T_{Ge}>T_{CoFe}$ (see Figs. 3g and 3h). This result clearly demonstrates another key feature of the SST and $\Delta\mu_{th}$ that the thermal spin signal reversed when ΔT is reversed.

In addition, this sign of the Hanle signal allows us to exclude other possible origins for the spin signal, for example, due to the spin-polarized hot-electron injection and conventional Seebeck effect, in the laser-heating experiment. The thermal excitation by the laser heating can result in a current flow in the Au pad and FM layer. Nevertheless, this electrical current cannot be an origin of the observed Hanle signal, since the sign of the observed $\Delta V_{TH,\,normal}$ (positive sign, see Fig. 4a) for the FM heating ($T_{CoFe}>T_{Ge}$) by the laser beam is opposite to that $\Delta V_{EH,\,normal}$ (negative sign) expected by the injection of spin-polarized hot-electron current into the Ge (see the bottom panel of Fig. 2a). This strongly suggests that the observed Hanle signal does not come from the electrical current in the injector.

Discussion

For a quantitative analysis, we have calculated the Hanle magnetothermopower (HMTP) (or Hanle magneto-Seebeck ratio (S_{Hanle}))[30] defined as the relative change of charge Seebeck coefficient (S) due to spin accumulation as follows:

$$S=\frac{V|_{I_{tunnel}=0}}{\Delta T},\ V|_{I_{tunneling}=0}=-\frac{L}{G}\Delta T+\frac{\gamma\Delta\mu_{th}}{(-2e)}\Delta T$$
$$=S_o\Delta T+\frac{\gamma}{(-2e)}S_{SST}\Delta T=V_{th}+\Delta V_{TH},\qquad(1)$$
$$S_{Hanle}\equiv\frac{S|_{B=0}-S|_{B(\Delta\mu=0)}}{S|_{B(\Delta\mu=0)}}=\frac{\Delta V_{TH}}{V_{th}},$$

where G is the electrical tunnel conductance, L is the thermoelectric tunnel conductance, S_o is the charge thermopower at zero $\Delta\mu_{th}$, and S_{SST} is the SST coefficient. Figure 5a shows the calculated HMTP (or S_{Hanle}) as a function of the P_{laser}. The HMTP value of $\Delta V_{TH,\,normal}/V_{th}$ is $\sim(+)7.0\%$ and remains almost constant with varying the P_{laser}. It is important to note that these values are $\sim$70 times larger than the maximum value ($\sim$0.1%) of Hanle magnetoresistance (HMR), defined as $\Delta V_{EH,\,normal}/V_{el}$, obtained by the electrical spin injection using the same contact *a* (see Fig. 2). This experimental result supports the theoretical proposition[30] that the thermal spin injection is more efficient than the electrical spin

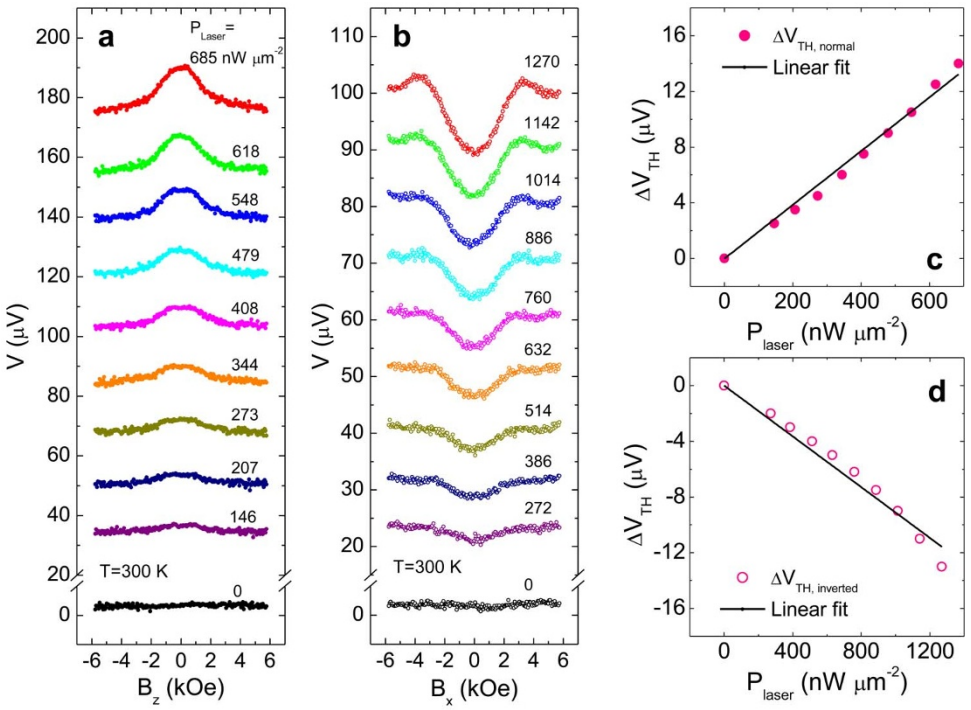

Figure 4 | Detection of thermal spin accumulation in Ge with heating FM. Obtained thermal spin signals under (a) perpendicular (B_z) and (b) in-plane (B_x) magnetic fields as a function of the laser power density (P_{laser}) at RT in the case of heating the FM ($\Delta T<0$). (c) $\Delta V_{TH,\,normal}$ and (d) $\Delta V_{TH,\,inverted}$ as a function of the laser power density (P_{laser}), together with a linear fit.

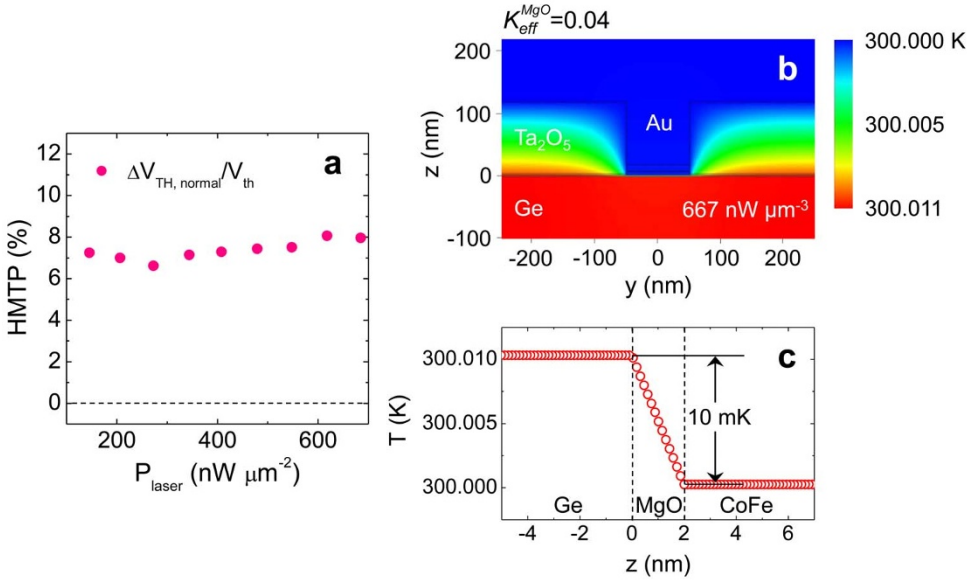

Figure 5 | Hanle magnetothermopower and Seebeck spin tunneling coefficient. (a) Calculated HMTP (or S_{Hanle}) as a function of the P_{laser}. (b) Simulated temperature distribution in a two-dimensional (2-D) cross-section and (c) temperature line scan cross the tunnel contact for the reasonable κ_{eff}^{MgO}($G_{th,eff}^{MgO}$) value of 0.04 (2×10^7) W m^{-1} K^{-1} (W m^{-2} K^{-1}) for the 2 nm-thick MgO, at the maximum $P_{heating}$ of 667 nW μm^{-3}.

injection for the tunnel contacts with the strong asymmetry in TSP and the moderate thermal interface resistance.

To estimate the value of S_{STT}, defined as $\Delta\mu_{th}/\Delta T$[30], the information of ΔT across the CoFe/MgO/Ge tunnel contact is required. We carried out the combined analyses using the one-dimensional (1-D) heat flow model[20] and simulation using a commercial finite element software (COVERTOR) to determine ΔT (see the Supplementary Information Note II). Both the 1-D heat flow model and commercial finite element simulation provide a similar magnitude of ΔT.

Figures 5b and 5c show the representative results of the simulated temperature distribution in a two-dimensional (2-D) cross-section and temperature line-scan cross the tunnel contact when heating the Ge with the maximum $P_{heating}$ of 667 nW μm^{-3}. Here we used a reasonable κ_{eff}^{MgO} value of 0.04 W m^{-1} K^{-1} (or a $G_{th,eff}^{MgO}$ of 2×10^7 W m^{-2} K^{-1}) for the 2 nm-thick MgO barrier. The possible range of ΔT across the tunnel contact is from 0.15 mK to 350 mK, and a reasonable ΔT is an order of 10 mK (see the Supplementary Information Note II for the detailed discussion). Using $\Delta\mu_{th}$ = 0.26 meV and ΔT =10 mK, the S_{STT} value is estimated to be 26 meV K^{-1} for the CoFe/MgO/*n*-Ge contact. If we use the largest ΔT of 350 mK, the S_{STT} goes down to 0.74 meV K^{-1}. These S_{STT} values are comparable to those of the $Ni_{80}Fe_{20}/Al_2O_3/SiO_2/p$-Si contact[20] but they are at least two orders of magnitude lager than the spin Seebeck coefficient (−3.8 μV K^{-1}) of the Co/Cu metallic system[33], which may be attributed to the different spin injection/detection efficiency and the different measurement scheme.

In conclusion, we have observed the thermal spin injection and accumulation in CoFe/MgO/*n*-type Ge contacts using local heating of electrodes by laser beam or electrical current. We demonstrate that the magnitude of thermally injected spin signal scales linearly with the power of local heating of electrodes, and its sign is reversed as we invert the temperature gradient. Based on the Seebeck spin tunneling theory, we have obtained a large Hanle magnetothermopower (HMTP) of about 7.0% and the Seebeck spin tunneling coefficient of larger than 0.74 meV K^{-1} in the CoFe/MgO/*n*-Ge contact at room temperature. This is attributed to the strong asymmetry in the TSP of the contact. Our experimental results demonstrate that the thermal spin injection is an efficient way of spin injection in SC.

Methods

Device fabrication. The single crystalline CoFe(5 nm)/MgO(2 nm)/*n*-Ge(001) tunnel structures were prepared by molecular beam epitaxy (MBE) system with a base pressure better than 2×10^{-10} torr. Prior to the deposition of CoFe/MgO layers, the composite *n*-Ge consisting of a heavily P-doped surface layer ($n_d\sim10^{19}$cm^{-3}at 300 K) and a moderately Sb-doped substrate ($n_d\sim10^{18}$cm^{-3}at 300 K) was formed by ion implantation technique. All layers were deposited by e-beam evaporation with a working pressure better than 2×10^{-9} torr. The MgO and CoFe layers were grown at 125°C and RT, respectively, and then the samples were subsequently annealed *in-situ* for 30 min at 300°C below 2×10^{-9} torr to improve the surface morphology and crystalllinity. Finally, the samples were capped by a 2 nm thick Cr layer at RT to prevent oxidation of the sample. The symmetric device (Fig. 1c) consisting of three tunnel contacts with lateral sizes of 100×300/100×300/100×300 μm^2 was prepared by using micro-fabrication techniques (e.g., photo-lithography and Ar-ion beam etching) for the thermal spin accumulation experiments. For the electrical isolation at the sides of the tunnel contacts, about 120 nm-thick Ta_2O_5(115 nm)/Al_2O_3(2 nm) layers were grown by sputtering technique. For the contact pads, 110 nm-thick Au(100 nm)/Ti(10 nm) layers were deposited.

1. Fert, A. Nobel lecture: Origin, development, and future of spintronics. *Rev. Mod. Phys.* **80**, 1517–1530 (2008).
2. Bauer, G. E. W., Saitoh, E. & van Wees, B. J. Spin caloritronics. *Nature Mater.* **11**, 391–399 (2012).
3. Jansen R. Silicon spintronics. *Nature Mater.* **11**, 400–408 (2012).
4. Žutić, I., Fabian, J. & Das Sarma, S. Spintronics: Fundamentals and applications. *Rev. Mod. Phys.* **76**, 323–410 (2004).
5. Fert, A. & Jaffrès, H. Conditions for efficient spin injection from a ferromagnetic metal into a semiconductor. *Phys. Rev. B* **64**, 184420 (2001).
6. Stevens, M. J. *et al.* Quantum Interference Control of Ballistic Pure Spin Currents in Semiconductors. *Phys Rev. Lett.* **90**, 136603–136606 (2003).
7. Dash, S. P., Sharma, S., Patel, R. S., de Jong, M. P. & Jansen, R. Electrical creation of spin polarization in silicon at room temperature. *Nature* **462**, 491–494 (2009).
8. Kioseoglou, B. T., Jonker, G., Hanbicki, A. T., Li, C. H. & Thompson, P. E. Electrical spin-injection into silicon from a ferromagnetic metal/tunnel barrier contact. *Nature Phys.* **3**, 542–546 (2007).
9. Lou, X. *et al.* Electrical detection of spin transport in lateral ferromagnet-semiconductor devices. *Nature Phys.* **3**, 197–202 (2007).
10. Jiang, X. *et al.* Highly spin-polarized room-temperature tunnel injector for semiconductor spintronics using MgO(100). *Phys. Rev. Lett.* **94**, 056601–056604 (2005).
11. Ando, Y. *et al.* Electrical injection and detection of spin-polarized electrons in silicon through Fe3Si/Si Schottky tunnel barrier. *Appl. Phys. Lett.* **94**, 182105–182107 (2009).
12. Sasaki, T., Oikawa, T., Suzuki, T., Shiraishi, M., Suzuki, Y. & Noguchi, K. Temperature dependence of spin diffusion length in silicon by Hanle-type spin precession. *Appl. Phys. Lett.* **96**, 122101–122103 (2010).
13. Ciorga, M., Einwanger, A., Wurstbauer, U., Schuh, D., Wegscheider, W. & Weiss, D. Electrical spin injection and detection in lateral all-semiconductor devices. *Phys. Rev. B* **79**, 165321 (2009).

14. Appelbaum, I., Huang, B. & Monsma, D. J. Electronic measurement and control of spin transport in silicon. *Nature* **447**, 295–298 (2007).
15. Jang, H. J. & Appelbaum, I. Spin polarized electron transport near the Si/SiO_2 interface. *Phys. Rev. Lett.* **103**, 117202–117205 (2009).
16. Kato, Y. K., Myers, R. C., Gossard, A. C. & Awschalom, D. D. Observation of the Spin Hall Effect in Semiconductors. *Science* **306**, 1910–1913 (2004).
17. Sih, V., Myers, R. C., Kato, Y. K., Lau, W. H., Gossard, A. C. & Awschalom, D. D. Spatial imaging of the spin Hall effect and current-induced polarization in two-dimensional electron gases. *Nature Phys.* **1**, 31–35 (2005).
18. Ando, K. *et al.* Electrically tunable spin injector free from the impedance mismatch problem. *Nature Mater.* **10**, 655–659 (2011).
19. Ando, K. & Saitoh, E. Observation of the inverse spin Hall effect in silicon. *Nat. Commun.* **3**, 629 (2012).
20. Le Breton, J. C., Sharma, S., Saito, H., Yuasa, S. & Jansen, R. Thermal spin current from a ferromagnet to silicon by Seebeck spin tunneling. *Nature* **475**, 82–86 (2011).
21. Jain, A. *et al.* Electrical and thermal spin accumulation in germanium. *Appl. Phys. Lett.* **101**, 022402–022404 (2012).
22. Jeon, K. R., Park, C. Y. & Shin, S. C. Epitaxial growth of MgO and CoFe/MgO on Ge(001) substrates by molecular beam epitaxy. *Cryst. Growth Des.* **10**, 1346–1350 (2010).
23. Jeon, K. R. *et al.* Temperature and bias dependence of Hanle effect in CoFe/MgO/ composite Ge. *Appl. Phys. Lett.* **99**, 162106–162108 (2011).
24. Johnson, M. & Silsbee, R. H. Interfacial charge-spin coupling: Injection and detection of spin magnetization in metals. *Phys. Rev. Lett.* **55**, 1790–1793 (1985).
25. Johnson, M. & Silsbee, R. H. Spin-injection experiment. *Phys. Rev. B* **37**, 5326–5335 (1988).
26. Lou, X., Adelmann, C., Furis, M., Crooker, S. A., Palmstrøm, C. J. & Crowell, P. A. Electrical detection of spin accumulation at a ferromagnet–semiconductor interface. *Phys. Rev. Lett.* **96**, 176603–176606 (2006).
27. Dash, S. P. *et al.* Spin precession and inverted Hanle effect in a semiconductor near a finite-roughness ferromagnetic interface. *Phys. Rev. B* **84**, 054410–054420 (2011).
28. Jeon, K. R. *et al.* Effect of spin relaxation rate on the interfacial spin depolarization in ferromagnet/oxide/semiconductor contacts. *Appl. Phys. Lett.* **101**, 022401–022405 (2012).
29. Jansen, R., Dash, S. P., Shrma, S. & Min, B. C., Silicon spintronics with ferromagnetic tunnel devices. *Semicond. Sci. Technol.* **27**, 083001 (2012).
30. Jansen, R., Deac, A. M., Saito, H. & Yuasa, S. Thermal spin current and magnetothermopower by Seebeck spin tunneling. *Phys. Rev. B* **85**, 094401–094408 (2012).
31. Parkin, S. S. P. *et al.* Giant tunnelling magnetoresistance at room temperature with MgO (100) tunnel barriers. *Nature Mater.* **3**, 862–867 (2004).
32. Yuasa, S., Nagahama, T., Fukushima, A., Suzuki, Y. & Ando, K. Giant room-temperature magnetoresistance in single-crystal Fe/MgO/Fe magnetic tunnel junctions. *Nature Mater.* **3**, 868–871 (2004).
33. Slachter, A., Bakker, F. L., Adam, J.-P. & van Wees, B. J. Thermally driven spin injection from a ferromagnet into a non-magnetic metal. *Nature Phys.* **6**, 879–883 (2010).

Acknowledgements

This work was supported by the DGIST R&D Program of the Ministry of Education, Science and Technology of Korea (11-IT-01); by the KIST institutional program (2E22732 and 2V02720) and by the Pioneer Research Center Program (2011-0027905); and by the KBSI grant no.T32517 for S-YP.

Author contributions

S.-C.S. supervised the project; K.-R.J. designed and conducted the experiments with the help of B.-C.M.; K.-R.J. prepared the samples; K.-R.J. and Y.-H.P. carried out the patterning process; K.-R.J. carried out the measurements; S.-Y.P., K.-D.L., H.-S.S. and Y.-H.J. contributed to the measurement setups; K.-R.J., B.-C.M. and S.-C.S. conducted theoretical analysis and wrote the manuscript.

Additional information

Supplementary information accompanies this paper at http://www.nature.com/scientificreports.

Competing financial interests: The authors declare no competing financial interests.

License: This work is licensed under a Creative Commons Attribution-NonCommercial-NoDerivs 3.0 Unported License. To view a copy of this license, visit http://creativecommons.org/licenses/by-nc-nd/3.0/

How to cite this article: Jeon, K. *et al.* Thermal spin injection and accumulation in CoFe/MgO/*n*-type Ge contacts. *Sci. Rep.* **2**, 962; DOI:10.1038/srep00962 (2012).